Ocean Engineering 117 (2016) 302–310

Contents lists available at ScienceDirect

Ocean Engineering

journal homepage: www.elsevier.com/locate/oceaneng

Experimental study on configuration optimization of floating breakwaters

Chun-Yan Ji [a], Xiang Chen [a,b], Jie Cui [a,*], Oleg Gaidai [a], Atilla Incecik [c]

[a] School of Naval Architecture and Ocean Engineering, Jiangsu University of Science and Technology, Zhenjiang 212003, China
[b] School of Naval Architecture, Ocean and Civil Engineering, Shanghai Jiao Tong University, Shanghai 200240, China
[c] Department of Naval Architecture, Ocean and Marine Engineering, University of Strathclyde, Glasgow, UK

ARTICLE INFO

Article history:
Received 15 October 2015
Accepted 1 March 2016
Available online 1 April 2016

Keywords:
Floating breakwater
Model experiments
Cylindrical
Porous
Mesh cage

ABSTRACT

In this paper, four types of floating breakwaters (FB) are proposed: cylindrical floating breakwater (CFB), porous floating breakwater (PFB), mesh cage floating breakwater type-I (MCFB-I) and mesh cage floating breakwater type-II (MCFB-II). The hydrodynamic performance of each type has been tested to identify the most effective configuration for wave attenuation. The experiment was conducted in a wave flume in which regular waves were produced. The incident and transmitted waves, the tensions in the mooring lines and the motion responses of all of the four types of floating breakwaters were measured. It is shown that all proposed types of floating breakwaters can effectively reduce transmitted wave amplitude. Among them the MCFB-I is seen to yield the most attenuating effect on incident wave amplitude.

1. Introduction

Floating breakwater is a type of harbor protection structure aimed at attenuating incoming wave. The reduction of transmitted wave energy is critical for the safety of other floating structures and ships.

Compared with the traditional bottom-fixed breakwaters, floating breakwaters has some advantages. Firstly, the cost of traditional bottom-fixed breakwater increases rapidly with water depth, while floating breakwaters offer a cheaper solution. Secondly, floating breakwater is friendlier to the ocean environment. Floating breakwaters can also be installed and disassembled more easily.

In 1811, a wood floating breakwater which is regarded as the first in the world was built in Plymouth Harbor. From then on, floating breakwaters were used to protect harbors, and their ability to decrease wave energy was proven. Since then people have been searching for a most effective configuration for floating breakwaters.

The most common configuration of floating breakwater is single pontoon. (Drimer et al., 1992; Sannasiraj et al., 1998; Abul-Azm and Gesraha, 2000; Koutandos et al., 2004; Gesraha, 2006; Elchahal et al., 2008; He et al., 2012, 2013; Peng et al., 2013; Koraaima and Rageh, 2013).

Based on single pontoon, floating breakwaters with double pontoons were designed, the inertia of which can be increased by adjusting the distance between the two pontoons without adding total weight. Both types of floating breakwaters mainly attenuate transmitted wave by reflecting incident wave, but double pontoon floating breakwater can also reduce waves between two floating pontoons. Williams and Abul-Azm (1997) investigated theoretically the hydrodynamic properties of a dual pontoon floating breakwater consisting of a pair of floating cylinders of rectangular section, connected by a rigid deck. The results reveal that the draft and spacing of the pontoons and the mooring line stiffness influence strongly the wave reflection properties of the structure. In 2006, Rahman et al. (2006) investigated a two-dimensional numerical estimation method of calculating dynamics of a pontoon type submerged floating breakwater and the forces acting on its mooring lines due to the wave action. Comparing the numerical with the experimental results, the validity of the numerical model and the good performance on wave energy dissipation is confirmed. In addition, the results illustrated that the clear space has a great effect upon responses of the structure; it not only changes the natural frequency of the structure, but causes heave motion to have a peak response in high frequency range. Another dual pontoon floating structure with a fish net for cage aquaculture is studied (Tang et al., 2011). The resonant responses of roll and tension RAO generally decrease as net depth increases, but the magnitudes of these changes are very small. The influence of net width on the dynamic motions is not only large, but also more complicated than the influence of net depth.

Both single and double pontoon floating breakwaters are reflective structures. Some other floating breakwaters are dissipative structures,

* Corresponding author. Tel.: +86 051189983009; mobile: +86 15050856887; fax: +86 051184404433.
E-mail address: cuijie2006@hotmail.com (J. Cui).

http://dx.doi.org/10.1016/j.oceaneng.2016.03.002
0029-8018/

where a certain amount of the incident energy dissipates by friction and turbulence, etc. Wang and Sun (2010) conducted an experimental study of a porous floating breakwater in 2010. The transmission coefficient decreased with the increase of both the width of the breakwater and the initial mooring force, and the dissipation of wave energy increases with the width of the breakwater. Another experimental study on the performance of a porous perpendicular pipe breakwaters was conducted by Shih (2010). They found that performance is greatly influenced by increased incident wave heights for shorter waves under identical pipe diameter and that larger pipe length is effective in reducing the reflection coefficient.

Traditional floating breakwaters are built of concrete and their strength is relatively low. Flexible structures are used on floating breakwaters to reduce cost. In 2008, Dong et al. (2008) conducted physical model tests to measure the wave transmission coefficient of the broad-net floating breakwater. The experimental results show that the board-net floating breakwater, which is a simple and inexpensive type of structure, can effectively protect fish and fish cages and may be adopted for aquaculture engineering in deep-water regions. Interaction of surface gravity waves with multiple vertically moored surface-piercing membrane breakwaters in finite water depth is analyzed based on the linearized theory of water waves (Karmakar et al., 2012). The comparison of the results for various fixed and moored edge conditions is analyzed for reflection and transmission coefficients. The conclusion showed that in the case of single surface-piercing membrane, with the increase in the length of the membrane and tension of the membrane the wave reflection increases and the presence of multiple floating breakwater helps in the reduction of wave height in the transmitted region. Hegde et al. (2008) studied the mooring forces in horizontal interlaced moored floating pipe breakwater with three layers. They found that the maximum force in the seaward side mooring for model with $S/D=4$ is lower compared to that for the breakwater model with $S/D=2$ (S is the spacing of pipes and D the diameter of pipe). Koraim (2013) conducted a new type of breakwater which consisted of one or more horizontal rows of half pipes suspended on supporting piles. With the number of rows increasing, the efficiency of breakwaters increases.

This paper introduces designs of four different floating breakwater (FB) models. Experimental study was conducted to measure the wave attenuating capability and hydrodynamic performance of each model. By analyzing the experimental results, the best structure configuration among the four types of floating breakwaters was determined.

2. Configuration design

The first FB model, i.e. model 1, is of a cylindrical double-pontoon configuration. Using the double pontoon configuration, the inertia of the FB can be increased to reduce its motion responses, and the FB can be built with larger width. Here a cylindrical FB structure is proposed consisting of two 4 m wide × 15.2 m long cylinders and nine 0.4 m diameter × 2 m long cylinders, as shown in Fig. 1. The material of the cylinders is reinforced concrete. This type of FB is referred to in this paper as the cylindrical floating breakwater.

Model 2 is a type of porous FB. The porous FB are well studied and proved efficient in wave attenuation. Due to exposure to wave load and sunlight, the traditional concrete FB is easy to crack and then sink due to flooding of inner enclose space. In this paper, a new structure design of the porous FB is introduced to prevent water leakage. The structure consists of two vertical plates, three longitudinal plates, three transverse plates and eight columns forming eight cabins. The holes are placed at the top parts of the vertical plates and the longitudinal and transverse plates. Four

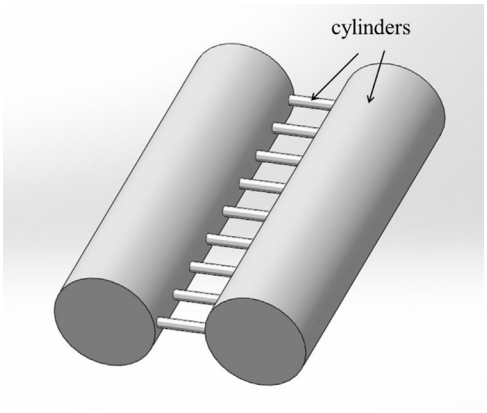

Fig. 1. Structure of Model 1: the cylindrical FB.

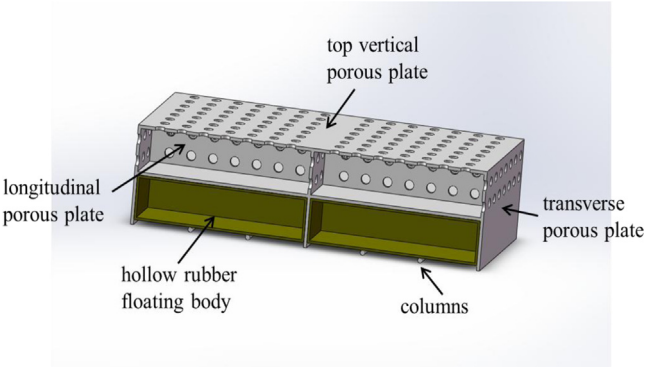

Fig. 2. Cross section of Model 2: the porous FB.

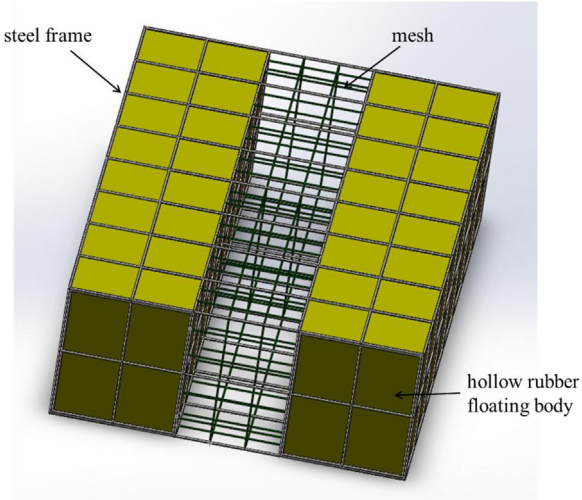

Fig. 3. Structure of Model 3: the mesh cage FB type-I.

hollow rubber floating bodies with long fatigue life are stuffed into the lower four cabins to provide buoyancy. The FB will remain afloat when one of the cabins is flooded. In the following contents Model 2 is referred to as the porous floating breakwater. The main structure of model 2 is shown in Fig. 2.

The structure configuration of Model 3 includes a cage and is referred to as the mesh cage FB type-I. It has a lower production cost than the two FB models introduced above. As shown in Fig. 3, the main frame of model 3 is made of steel. Two hollow rubber floating bodies are placed at the front and back of the floating breakwater, to

keep floatation and reflect incoming waves. Between the two bodies, meshes are installed on the steel to dissipate wave energy.

Model 4 also has a cage and is referred to as mesh cage FB type-II in Fig. 4. In order to increase fatigue life, the rubber floating body is placed below the wave surface on the steel frame. Meshes are installed at the top part of the frame.

3. Experimental setup

3.1. Experimental facilities and equipment

Figs. 5 and 6 demonstrates the experimental setup. A series of experiments are conducted in the wave flume of the Hydraulics Modeling Laboratory of Ocean University of China, suitable for two-dimensional hydrodynamic tests. The wave flume is 60 m long, 3.0 m wide and 1.5 m deep. For this study, the flume width was reduced to 0.8 m, in accordance with the experimental scale. A piston-type wave-maker was installed at one end of the flume. The wave-absorbing beach was located at the opposite end to reduce the wave reflection.

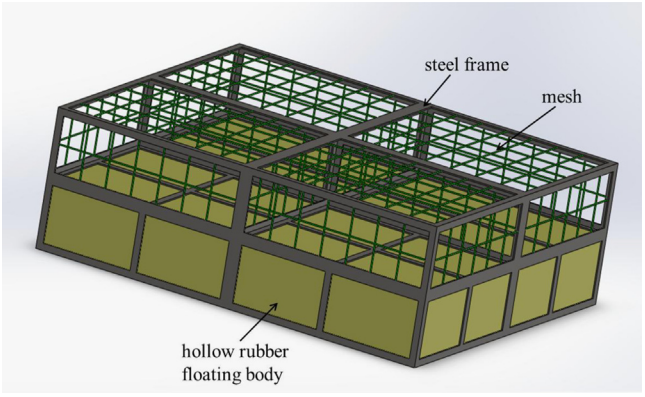

Fig. 4. Structure of Model 4: the mesh cage FB type-II.

As shown in Fig. 5, the model is moored by catenary lines. Each mooring line is made of stainless steel and has a length of 1.6 m with a line density of 0.63 kg/m. Two one-dimensional strain gauges are used to record the tensile stress of the mooring line.

Measurements of the incident wave height and the transmitted wave height is conducted with 5 wave gauges placed at different places in the flume. The distances between the wave gauges are listed in Table 1.

3.2. Experimental models

In order to find the most efficient configuration, four FB types are analyzed in this paper. For the purpose of consistency of model comparison, the main dimensions of each model are chosen to be the same (Figs. 7 and 8).

Model 1 is the cylindrical FB consisting of two 0.2 m diameter cylinders and nine 0.02 m diameter cylinders as shown in Fig. 9.

Model 2 is the porous FB which is shown in Fig. 10. Three porous longitudinal plates, three porous transverse plates, two porous vertical plates and eight columns are combined into model 2.

As shown in Figs. 11 and 12, Model 3 and 4 are the type-I and type-II mesh cage FBs, respectively. The frames of Model 3 and 4 are all fabricated with steels. Two floating bodies are placed at the front and the back of Model 3, and meshes are installed between the floating bodies. One floating body is installed at the bottom of Model 4 and meshes are installed at the top part.

Main parameters of the four models are listed in Table 2.

Table 1
Distances between wave gauges.

Wave gauges	Distances (cm)
WG1 and WG2	460
WG2 and WG3	40
WG3 and WG4	650
WG4 and WG5	40

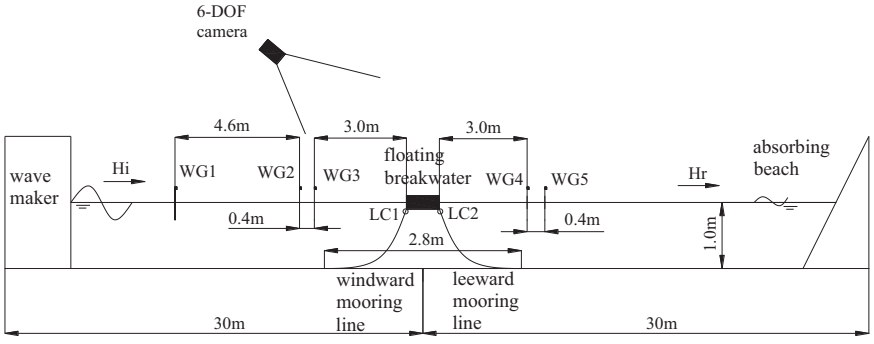

Fig. 5. Floating breakwater installation in the flume.

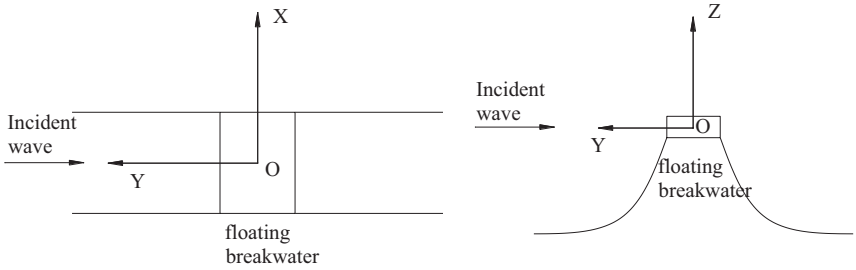

Fig. 6. The coordinate system of breakwater.

Fig. 7. Model 1.

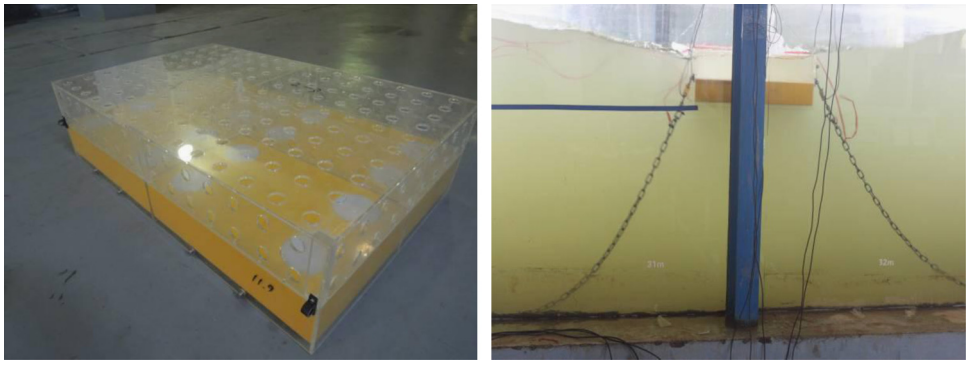

Fig. 8. Model 2.

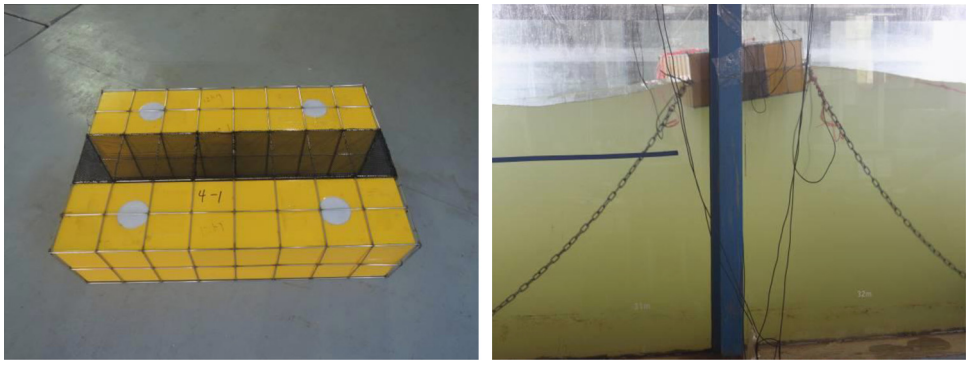

Fig. 9. Model 3.

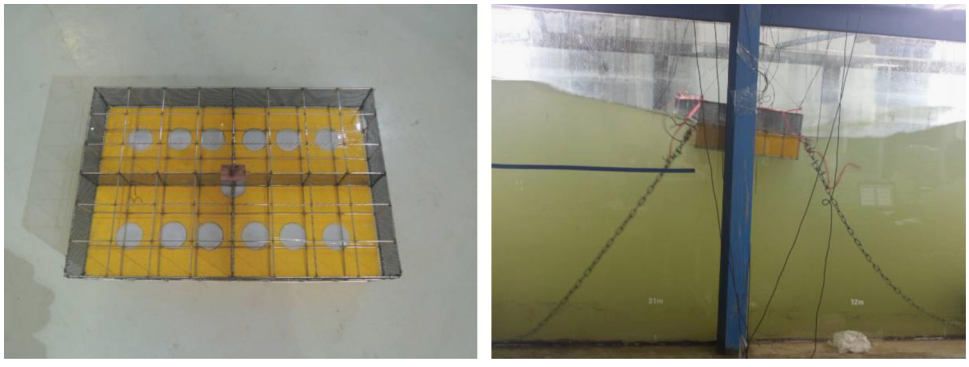

Fig. 10. Model 4.

3.3. Model scale and experimental conditions

In accordance with the dimensions of experimental facilities and the tested wave conditions, the scale is 1:20. In all experiments, the water depth is 1 m. Therefore, the prototype water depth is 20 m. The regular wave periods range from 0.9 to 1.4 s, and the wave heights from 0.1 to 0.2 m. Details are presented in Table 3.

4. Results and discussions

This paper employs the two-point method presented by Goda and Suzuki (1976). This method separates the amplitudes of incident wave (A_i) and reflected wave (A_r) by the measured surface elevations. One can separate the amplitude of incident wave (A_i) from WG2-3 and obtain the amplitude of transmitted wave (A_t)

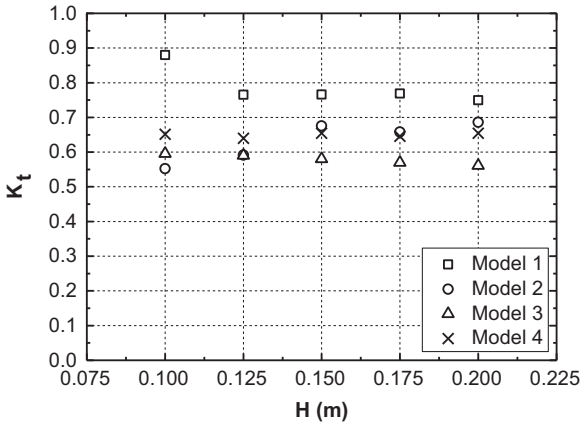

Fig. 11. Transmission coefficients of the four models (T=1 s).

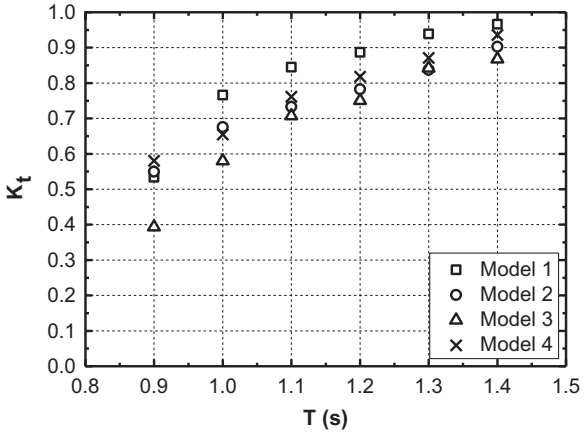

Fig. 12. Transmission coefficients of the four models (H=0.15 m).

Table 2
Main parameters of four models.

	Length (mm)	Width (mm)	Height (mm)	Draft (mm)	Mass (kg)	Roll inertia (kg m^2)	Gravity center above bottom (mm)
Model 1	760	500	200	100	19.1	0.474	100
Model 2	760	500	200	100	28.0	0.647	69
Model 3	760	500	200	100	19.1	0.558	100
Model 4	760	500	200	100	27.3	0.554	52

from WG4-5. The transmission coefficient (K_t) is defined as A_t/A_i. Besides, the amplitude of each motion response was monitored by the 6-DOF camera installed at the front of FB. The peak values of forces acting on the windward and leeward lines were recorded by strain gauges.

4.1. Wave transmission coefficients

Fig. 11 shows the relationship between the transmission coefficients and the wave height for the four models when the wave period is 1.0 s.

As shown in Fig. 11, the transmission coefficients of Model 1 and 3 slightly decrease with the increase of wave height. As we know, higher wave leads to intense movement that will improve wave reflection and increase wave energy dissipation. But K_t of Model 2 increases with the wave height. For Model 2, due to porosity of the plates, higher wave will lead more waves to flow into the top part of the model. This part of water adds to the weight of Model 2 so that a large part of Model 2 will sink below the waterline. Therefore more waves will be transmitted beyond Model 2. K_t of Model 4 is nearly unchanged. Since higher wave results in greater reflection and dissipation, more waves will transmit beyond the floating body of Model 4. Comparing the four models, the transmission coefficient K_t is found to be the smallest for Model 3 and the largest for Model 1.

Table 3
Experimental test conditions.

H (m)	T (s)
0.1	1.0
0.125	1.0
0.15	0.9, 1.0, 1.1, 1.2, 1.3, 1.4
0.175	1.0
0.2	1.0, 1.1, 1.2, 1.3, 1.4

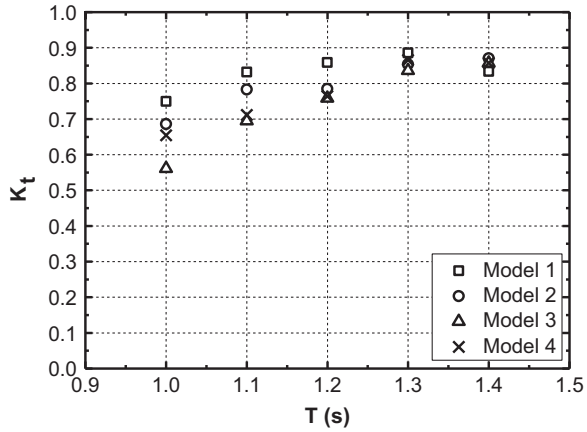

Fig. 13. Transmission coefficients of the four models (H=0.2 m).

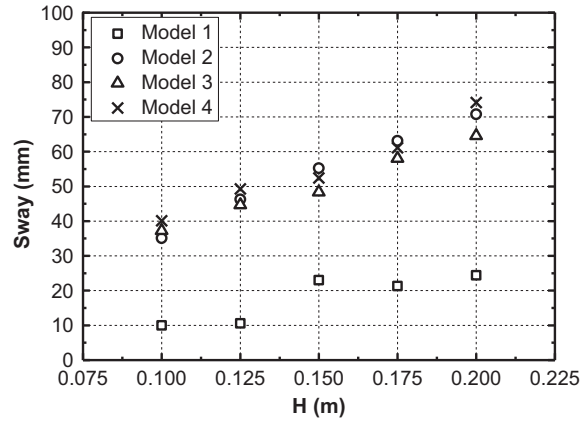

Fig. 14. Sway motion of the four models (T=1 s).

Figs. 12 and 13 reveal changes in transmission coefficients against the wave period for the four models when the wave height is 0.15 m and 0.2 m.

As seen in Figs. 12 and 13, the transmission coefficients of all models increase with the increase of the wave period. Model 3 transmission coefficient K_t is found to be the smallest. As H=0.15 m and T=0.9 s, K_t of Model 3 is about 20% smaller than for the other three models. The windward area of Model 3 is the largest among all four models, therefore it exhibits stronger wave reflection. In addition, wave energy is dissipated by destroying

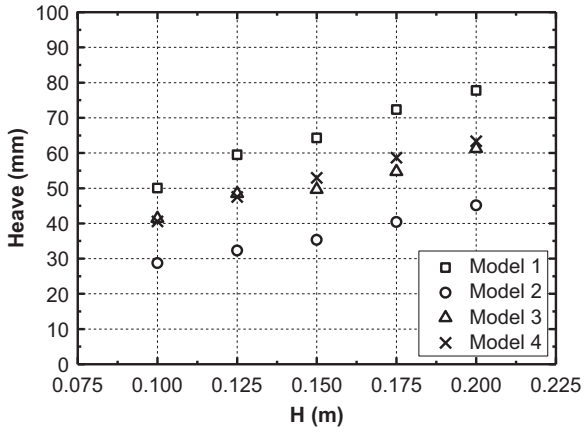

Fig. 15. Heave motion of the four models (T=1 s).

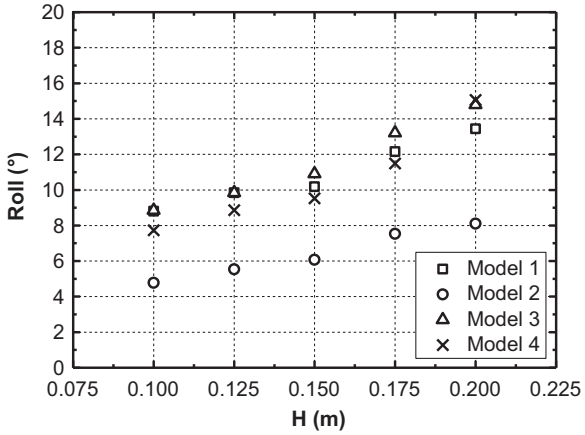

Fig. 16. Roll motion of the four models (T=1 s).

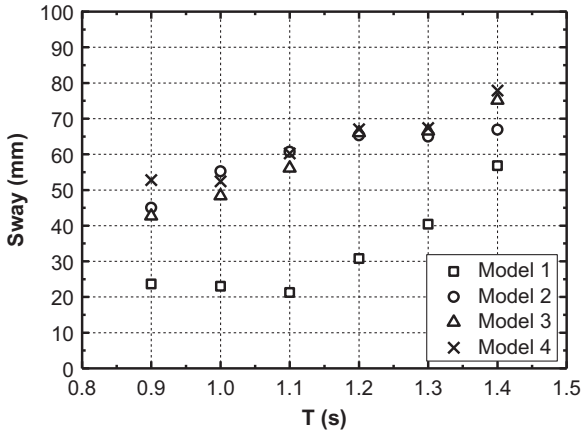

Fig. 17. Sway motion of the four models (H=0.15 m).

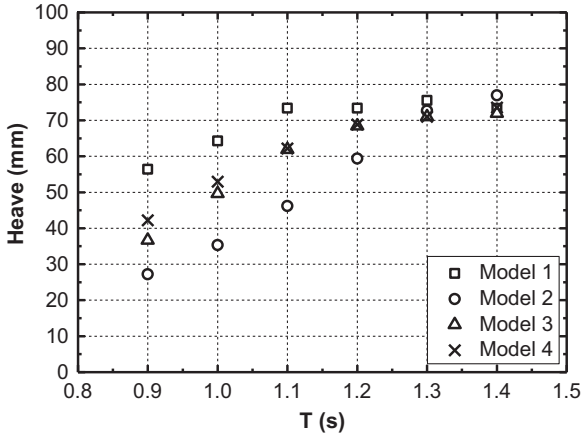

Fig. 18. Heave motion of the four models (H=0.15 m).

particle orbit and the flow of water through the mesh holes of Model 3.

Above all, Model 3 shows more wave attenuation than the other three models.

4.2. Motion responses

With the wave period being 1.0 s, Figs. 14–16 show for the four models the variation of motion responses with the wave height. Figs. 17–22 show for the four models the variations of motion responses with the wave period, given the wave height 0.15 m and 0.2 m.

As shown in Figs. 14–16, the motion responses of all models increase with the wave height. Comparing the four models, the heave and roll motions of Model 2 are the smallest. The reason is that due to the porous plates, Model 2 submerge in the water, which results in an increase of weight, inertia and damping for Model 2. Therefore its heave and roll motions damped. The sway motion of Model 1 is the smallest. At the same time, the heave motion of Model 1 is the largest. The responses of Model 3 and 4 are nearly similar.

As seen in Figs. 17, 18, 20 and 21, the sway and heave motions increase with the increase of the wave period. The sway motion of Model 1 is still the smallest. But the growth rate of sway motion is rapid for Model 1. Observing the results carefully, one will find that when wave period T is small, the sway motion of Model 1 is far smaller than other three models. But when T is up to 1.4 s, the sway motion of Model 1 is close to other three models.

Figs. 19 and 22 show the variation of roll motion with the wave period for the four models. When H=0.15 m, the roll motions of Model 3 and 4 decrease with the increase of wave period, but Model 1 is nearly unchanged. As H=0.2 m, the roll motion of Model 1 increase with the increase of wave period, but that of Model 3 and 4 stays nearly unchanged.

Overall, the sway motion of Model 1 is the smallest and the heave and roll motions of Model 2 are the smallest. The motion responses of Model 3 and 4 are the same.

4.3. Mooring forces

Figs. 23 and 24 show the variations of mooring forces with the increase of wave height for the four models when the wave period is 1.0 s.

As shown in Figs. 23 and 24, the mooring forces of Model 1, 3, 4 increase with the increase of the wave height and the mooring forces of Model 2 are nearly unchanged. The mooring forces of Model 1 are the biggest among the four models. The higher the wave, the greater the force acting on model. So, the intension of mooring force will increase. But for model 2, the sinking causes the mooring lines to slack. In addition, the movement of submerged model 2 is slight. These two reasons result in the decrease of the mooring forces with wave height.

Figs. 25–28 reveal changes of mooring forces against the wave period for the four models as the wave height is 0.15 m and 0.2 m.

The forces acting on the windward line for the four different models changes in different patterns. As T=1.2 s, F_w of Model 1 is the smallest. F_ws of Model 2 and 4 increase with the increase of wave period. When H=0.15 m, F_w of Model 3 decreases when the wave period increases. However, as H=0.2 m, F_w of Model 3 stays nearly unchanged for different wave periods. For the force acting

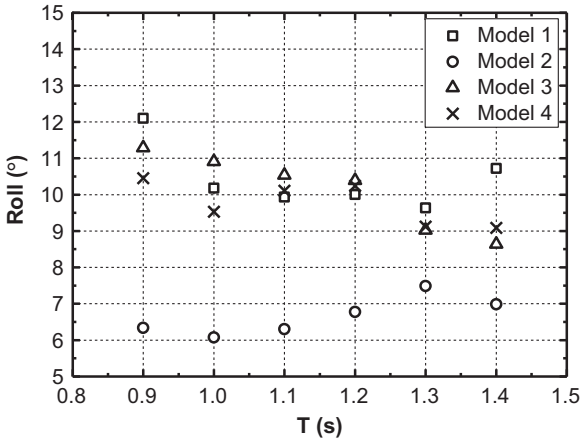

Fig. 19. Roll motion of the four models (H=0.15 m).

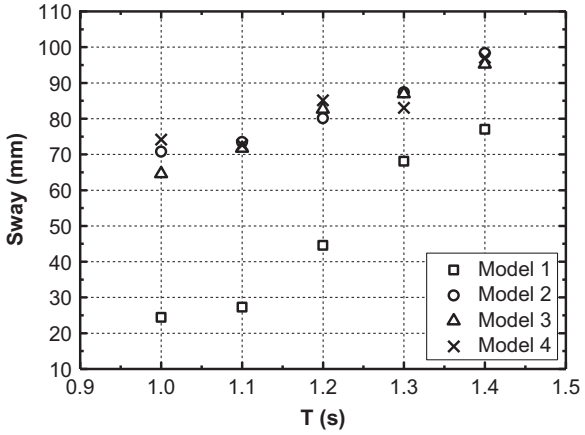

Fig. 20. Sway motion of the four models (H=0.2 m).

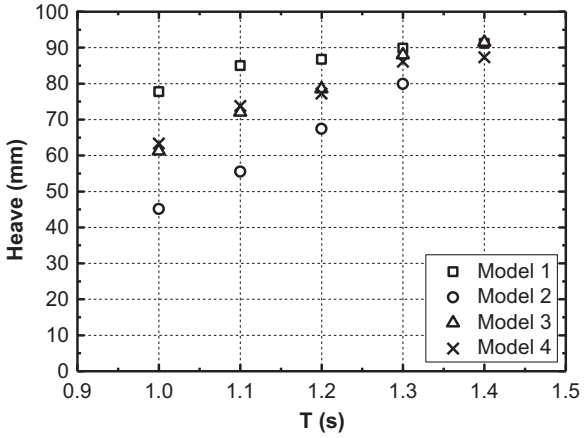

Fig. 21. Heave motion of the four models (H=0.2 m).

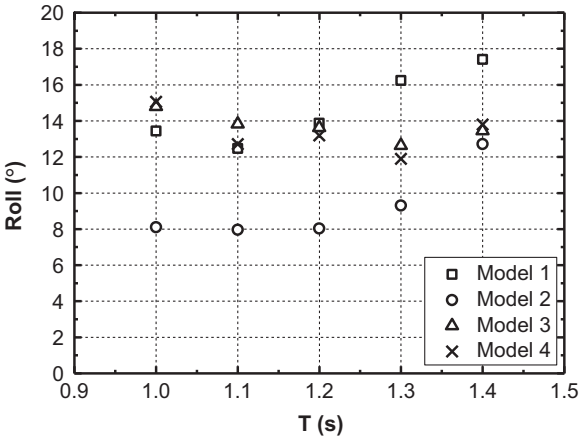

Fig. 22. Roll motion of the four models (H=0.2 m).

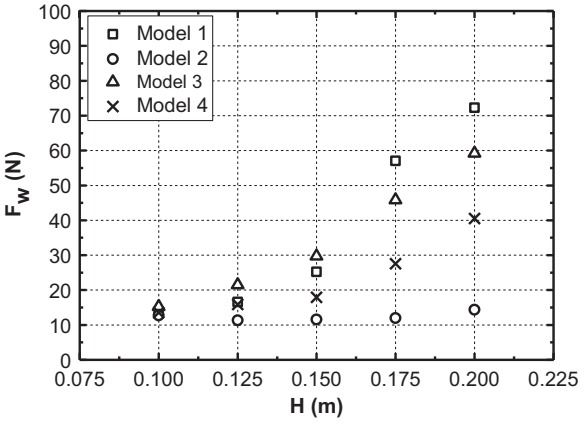

Fig. 23. Forces acting on the windward mooring lines of the four models (T=1 s).

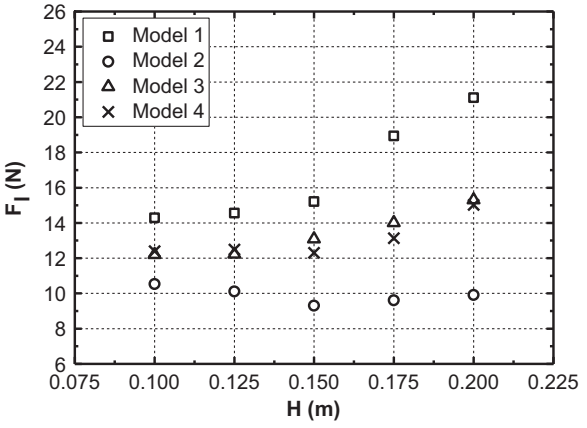

Fig. 24. Forces acting on the leeward mooring lines of the four models (T=1 s).

on the leeward line, F_l of Model 2 is nearly unchanged and for the other three models it increases with the increase of wave period.

Comparing between four models, the mooring forces of Model 2 are the smallest.

5. Conclusions

In this paper, four types of breakwater are proposed. A series of regular wave experiments were carried out to find the configuration that gives most wave attenuation. According to results, the following conclusions are drawn:

1) All four models reduce transmitted wave. Due to the bigger windward area and the mesh-induced energy dissipation, the mesh cage FB type-I (Model 3) reflects waves and dissipates wave energy more effectively than the other three models.
2) The porous FB (Model 2) allows water to flow into the top part of the FB, which causes the FB to sink. Therefore the wave transmission increases. However, in this way, the weight, inertia and motion damping of the porous floating breakwater are

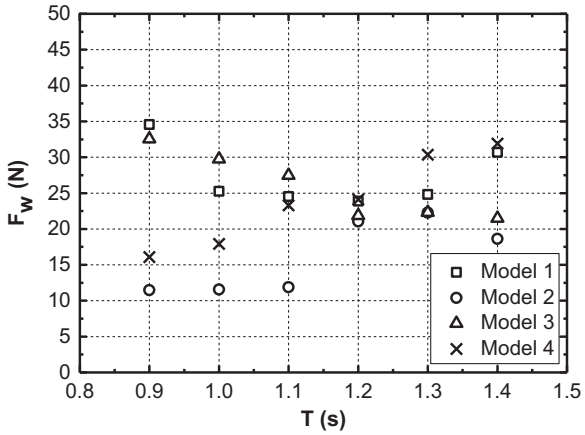

Fig. 25. Forces acting on the windward mooring lines of the four models (H=0.15 m).

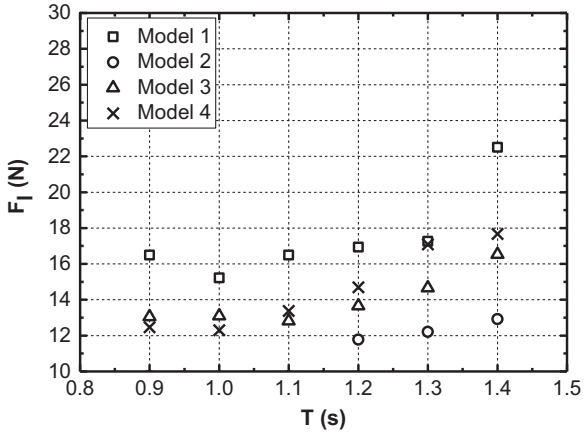

Fig. 26. Forces acting on the leeward mooring lines of the four models (H=0.15 m).

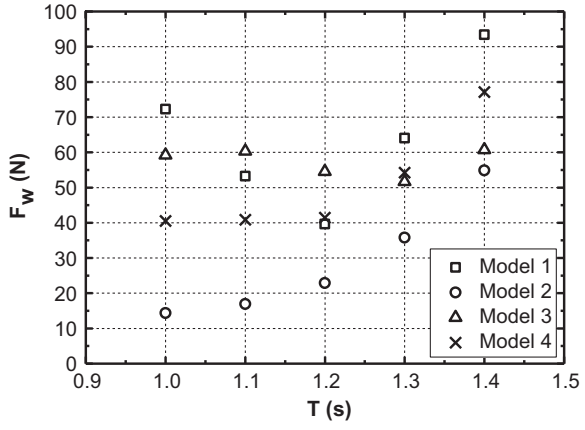

Fig. 27. Forces acting on the windward mooring lines of the four models (H=0.2 m).

improved so much that the heave and roll motions are smaller than that of the other types. The mooring forces of the porous floating breakwater are also found to be the smallest among all the four types of FBs.

3) The cylindrical FB (Model 1) has the weakest wave attenuating capability among all four types of FBs. In addition, its sway motion and mooring forces are the largest.
4) The hollow top structure of the mesh cage FB type-II (Model 4) is the same with that of the porous FB. These two types of FB all allow water into the top part of them so that they will sink under waterline. Therefore, the wave attenuation and the mooring forces are similar among them.

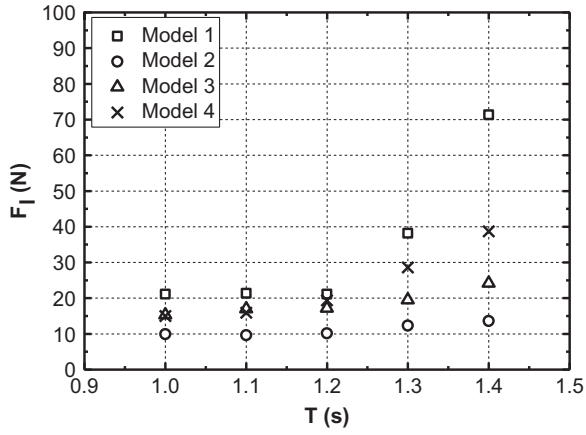

Fig. 28. Forces acting on the leeward mooring lines of the four models (H=0.2 m).

Above all, the mesh cage FB type-I has the best performance in wave attenuation; the motion responses and the mooring forces of the porous FB are the smallest. It may be possible to further improve the hydrodynamic performance of the mesh cage FB type-I with porous structures, but it is difficult to place holes on rubber bodies. Further researches are needed to find better configurations of floating breakwaters.

Acknowledgment

This study was supported financially by the National Natural Science Foundation of China, China (Grant nos. 51579122, 51379095 and 51409129) and the National Basic Research Program of China (973 Program; Grant no. 2013CB36100) and Natural Science Found of Jiangsu province (BK20150011 and BK20140504).

References

Abul-Azm, A.G., Gesraha, M.R., 2000. Approximation to the hydrodynamics of floating pontoons under oblique waves. Ocean Eng. 27, 365–384.
Dong, G.H., Zheng, Y.N., Li, Y.C., Teng, B., et al., 2008. Experiments on wave transmission coefficients of floating breakwaters. Ocean Eng. 35, 931–938.
Drimer, N., Agnon, Y., Stiassnie, M., 1992. A simplified analytical model for a floating breakwater in water of finite depth. Appl. Ocean Res. 14, 33–41.
Elchahal, G., Younes, R., Lafon, P., 2008. The effects of reflection coefficient of the harbour sidewall on the performance of floating breakwaters. Ocean Eng. 35, 1102–1112.
Goda, Y., Suzuki, Y., 1976. Estimation of incident and reflected waves in random wave experiments. In: Proceedings of the 15th International Conference on Coastal Engineering. ASCE, pp. 828–845.
Sannasiraj, S.A., Sundar, V., Sundaravadivelu, R., 1998. Mooring forces and motion responses of pontoon-type floating breakwaters. Ocean Eng. 25 (1), 27–48.
Hegde, A.V., Kamath, K., Deepak, J.C., 2008. Mooring forces in horizontal interlaced moored floating pipe breakwater with three layers. Ocean Eng. 35, 165–173.
He, F., Huang, Z.H., Adrian, W.-K.L., 2012. Hydrodynamic performance of a rectangular floating breakwater with and without pneumatic chambers: an experimental study. Ocean Eng. 51, 16–27.
He, F., Huang, Z.H., Adrian, W.-K.L., 2013. An experimental study of a floating breakwater with asymmetric pneumatic chambers for wave energy extraction. Appl. Energy 106, 222–231.
Koraim, A.S., 2013. Hydrodynamic efficiency of suspended horizontal rows of half pipes used as a new type breakwater. Ocean Eng. 64, 1–22.
Koraima, A.S., Rageh, O.S., 2013. Effect of under connected plates on the hydrodynamic efficiency of the floating breakwater. China Ocean Eng. 28 (3), 349–362.
Karmakar, D., Bhattacharjee, J., Soares, C.G., 2012. Scattering of gravity waves by multiple surface-piercing floating membrane. Appl. Ocean Res. 39, 40–52.

Koutandos, E.V., Karambas, Th.V., Koutitas, C.G., 2004. Floating breakwater response to waves action using a Boussinesq model coupled with a 2DV Elliptic Solver. J. Waterw. Port Coast. Ocean Eng., 243–255.

Gesraha, M.R., 2006. Analysis of Π shaped floating breakwater in oblique waves: I. Impervious rigid wave boards. Appl. Ocean Res. 28, 327–338.

Rahman, M.A., Mizutani, N., Kawasaki, K., 2006. Numerical modeling of dynamic responses and mooring forces of submerged floating breakwater. Coast. Eng. 53 (10), 799–815.

Shih, R.S., 2010. Experimental study on the performance characteristics of porous perpendicular pipe breakwaters. Ocean Eng. 50, 53–62.

Tang, H.J., Huang, C.C., Chen, W.M., 2011. Dynamics of dual pontoon floating structure for cage aquaculture in a two-dimensional numerical wave tank. J. Fluids Struct. 27, 918–936.

Williams, A.N., Abul-Azm, A.G., 1997. Dual pontoon floating breakwater. Ocean Eng. 24 (5), 465–478.

Wang, H.Y., Sun, Z.C., 2010. Experimental study of a porous floating breakwater. Ocean Eng. 37, 520–527.

Peng, W., Lee, K.H., Shin, S.H., Mizutani, N., 2013. Numerical simulation of interactions between water waves and inclined-moored submerged floating breakwaters. Coast. Eng. 82, 76–87.